# Experiment 7: Mach-Zehnder

**Rory Fox**
**Lab Partner: Jordan Walsh**

PY4113 Report

School of Physics
University College Cork
Ireland
Septermber 2023

# Contents

# Chapter 1

# Introduction and Motivation

The purpose of this experiment was to gain experience with common aspects of optical telecommunication, electro-optic modulators, DFB lasers, as well as the theory assosciated with the spectrum and real-time behaviour of the modulated signal In this experiment, the behaviour of a DFB laser was characterised for different points of operating current and temperature. Interesting results regarding the temperature sensitivity of the laser spectrum were verified. Using the laser and a Mach-Zehnder modulator (MZM), the transfer function of the MZM was measured in agreement with the theoretical model. By applying an RF voltage to the modulator, the optical spectrum and time series data for the modulated signal were investigated for the critical points of DC operation (maximum power, minimum power and quadrature). The evenly spaced optical sidebands at integer multiples of the modulating frequency (so-called "Bessel Tones") were observed. The frequency doubling and higher harmonic terms which would be expected in the FFT of the time series were observed, and compared with a simulated model.

# Chapter 2

# Fundamentals

The fundamental process in this experiment was the modulation of laser light by a Mach-Zehnder modulator (MZM). A MZM is a device where light is split into two seperate arms, and a relative phase difference is introduced between the two by means of a difference in refractive index between the arms. When the two arms recombine, the two waves interfere due to the phase difference.

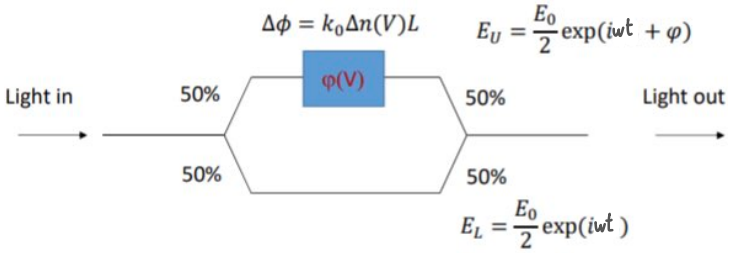


Figure 2.1: Basic Schematic for a simple Mach-Zehnder Inferometer

By considering the superposition of $E_U$ and $E_L$, we determine that the electric field up to some phase constant is

$$E_{out} = E_0 cos(\frac{\Delta\phi}{2}) e^{i(\omega t + \frac{\Delta\phi}{2})} \tag{2.1}$$

Where $\Delta\phi$ is the relative phase difference between the two arms.

With corresponding intensity

$$I_{out} = I_0 cos^2(\frac{\Delta\phi}{2}) \tag{2.2}$$

To enable the MZM to be used as a modulator, it was neccessary to be able to tune the phase difference between the two arms. This was accomplished by applying a voltage to the Lithium Niobate waveguide. According to the Pockels effect, "when certain kinds of birefringent crystal are placed in an electric field, their indices of refraction are altered by the presence of the field" [3]

Assuming the phase difference to be due to a difference in refractive index

$$\Delta\phi = \frac{2\pi L \Delta n_{eff}}{\lambda_0}$$

If one takes $\Delta n_{eff}$ to be a function of the biasing voltage $\Delta n_{eff}(V)$, one can rewrite the real part of equation 2.1 as a function of V.

For a more complete treatment of the mathematics behind the Mach-Zehnder modulator and the various higher order optical sidebands observed, the results of Dar and Ahmad may be consulted [1]. For the purposes of this report a more heuristic motivation for the sidebands will be given.

If the voltage is now considered to be the DC biasing voltage plus some additional RF voltage with amplitude $V_0$ and frequency $f_m$, the real component of the Electric Field may be written in terms of a sum of objects of the form

$$cos(2\pi f_c t + V_0 sin(2\pi f_m t))$$

This mathematical object $cos(f_1 t + \beta sin(f_2 t))$, can be expressed in terms of the Bessel functions and single cosines using the following relations

$$\cos(z\sin\theta) = J_0(z) + 2\sum_{k=1}^{\infty} J_{2k}(z)\cos(2k\theta)$$

$$\sin(z\sin\theta) = 2\sum_{k=0}^{\infty} J_{2k+1}(z)\sin((2k+1)\theta)$$

$$J_{-n}(z) = (-1)^n J_n(z)$$

Which were taken from Abramowitz and Stegun [2]

Using these identities, we can write

$$cos(2\pi f_c t + V_0 sin(2\pi f_m t)) = \sum_{k=-\infty}^{k=\infty} J_k(V_0) cos(2\pi(f_c + k f_m)t) \tag{2.3}$$

It would be expected to observe sidebands on either side of the carrier peak at integer multiples of the modulation frequency $f_m$. These are the so-called Bessel tones of the modulated signal.

The laser used was a distributed feedback laser (DFB).

DFB lasers, commonly used in telecommunications, ensure clean single-mode operation, unlike Fabry-Perot (FP) or Distributed Bragg Reflector (DBR) lasers. FP lasers rely on multibeam interference between mirrors, allowing periodic bands of wavelengths to pass [3]. This makes them susceptible to mode-hopping to another wavelength, as temperature or current variations may result in another FP mode being amplified. Replacing one FP mirror with a Bragg grating creates a DBR laser, narrowing the band of passed wavelengths. DFB lasers incorporate the grating throughout the cavity, enhancing stability against fluctuations.

For stable operation, DFB lasers are temperature-controlled using a Thermoelectric cooler (TEC) based on the Peltier effect. Applying an electric field to a thermoelectric

material transports heat, allowing for precise temperature control. However, driving a current in the material also generates ohmic heating. By selecting materials of suitable Peltier coefficient, and adjusting the current, the material can therefore either be heated or cooled, ensuring stable temperature.[4]

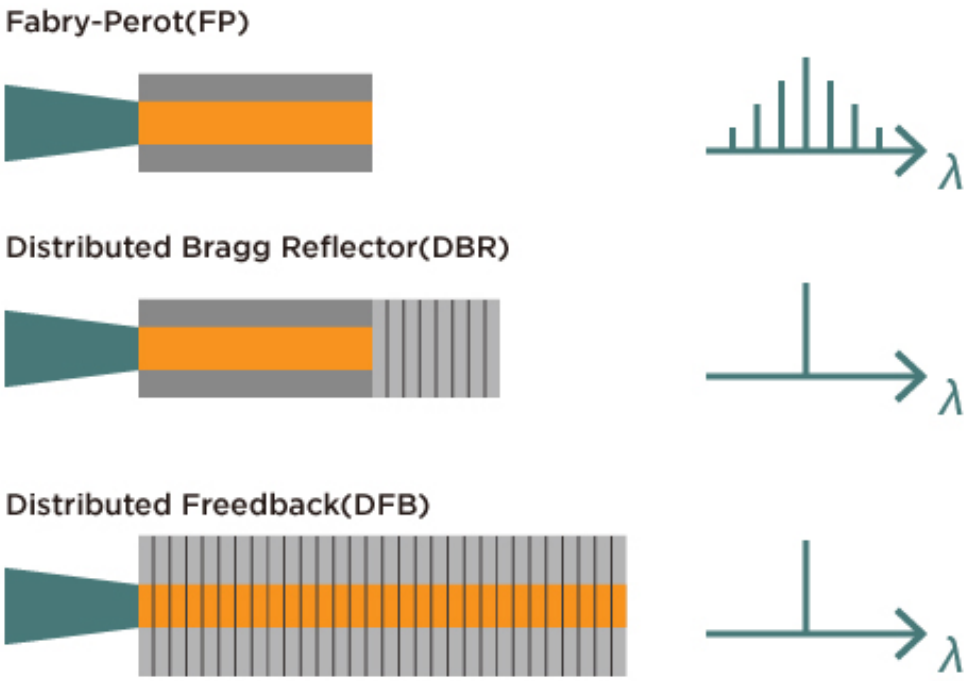


Figure 2.2: Figure showing spectra of ideal Fabry Perot, DFB and DBR lasers.

# Chapter 3

# Experiments, Results & Discussions

For brevity's sake the equipment specific instructions from the lab manual is not reproduced here. However, a general overview of the experiments carried out and any modifications is provided. The sources of error due to measurement in this experiment were negligible compared to larger, uncontrollable errors (transfer function drift etc), and were not particularly significant to the main goal of observing the behaviour of the modulated signal. Therefore no detailed error analysis was performed. Sources of error will be discussed in the results, where applicable.

## 3.1 Characterisation of LI Curve


In this measurement, the laser was directly connected to the power meter which was set to read in Watts. The temperature was kept constant at 25.0°C for the entirety of the experiment. Starting from zero current, power was recorded at various current increments, generating a power-current (LI) plot. The procedure was repeated for three consecutive measurements without changing apparatus to assess power meter uncertainty. Subsequently, fiber connections were disconnected and replaced to evaluate uncertainties related to coupling.

Although it was not necessary here, to convert from dBm to mW, there is the formula

$$P_{mW} = 1mW \cdot 10^{\frac{P_{dBm}}{10}}$$

dBm is a logarithmic scale for power relative to 1mW, it can be useful as it is able to express both very large and very small powers in a short hand form. A 3dB reduction is proportional to a 50% decrease in power.

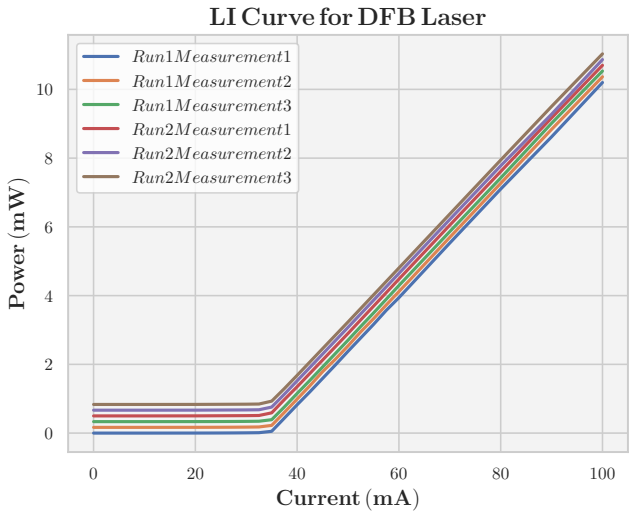


Figure 3.1: LI Curves measured for the DFB laser, small vertical offset added to each measurement for readability. In raw data curves sat on top of each other

The threshold current was calculated using an average of the LI Curves, a second derivative test was performed on the LI curve to determine the threshold current. This gave

$$\mathbf{I_{threshold} = 35mA}$$

As well as this, a linear fit of the lasing section of the LI curve gives the current to generate 10mW power.

$$\mathbf{I_{10mW} = 98.71mA}$$

From the maximum power of the laser, the NOHD was calculated according to the formula

$$NOHD = \sqrt{\frac{1}{\phi}((\frac{4\phi}{\pi MPE}) - a^2)}$$

Where $a$ is the aperture, $MPE$ is the maximum permitted exposure, and $\phi$ is the divergence angle.

According to UCC's guidlines, for a 1500nm laser, the MPE is $1000 W m^{-2}$ Assuming a divergence angle of $\phi \approx \frac{2\lambda}{\pi\omega_0} = 0.19 rad$ This gives a NOHD of 0.035m = 3.5cm

Additionally, power was measured at a fixed current across various temperatures to analyze temperature fluctuations' impact on the laser output.

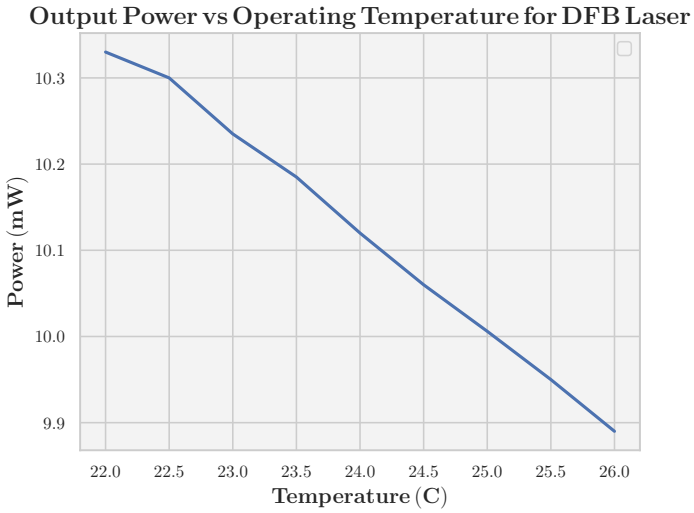


Figure 3.2: Laser output power at various temperature set points of the TEC

It was observed that at lower temperatures, the output power of the laser increased, and that there was an approximately linear decline moving towards higher temperatures.

## 3.2 Characterisation of the laser spectrum

### 3.2.1 Procedure


The laser was connected directly to the Optical Spectrum analyser (OSA). The current was set to a number of values before, about and after the threshold (determined from LI curves generated previously). The spectrum was also measured at several different temperatures for a fixed current to observe any differences to the spectrum due to temperature fluctuations

### 3.2.2 Results

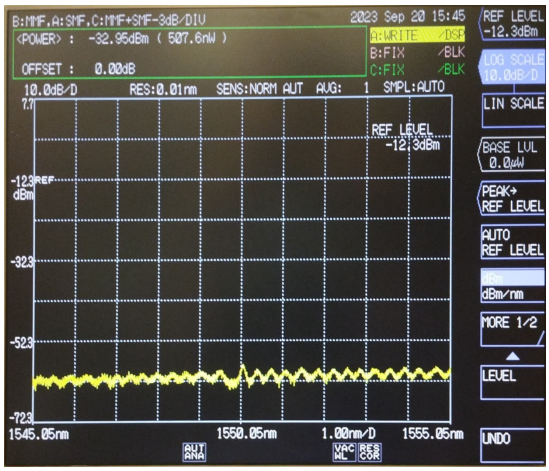


(a) $I = 27.5mA$

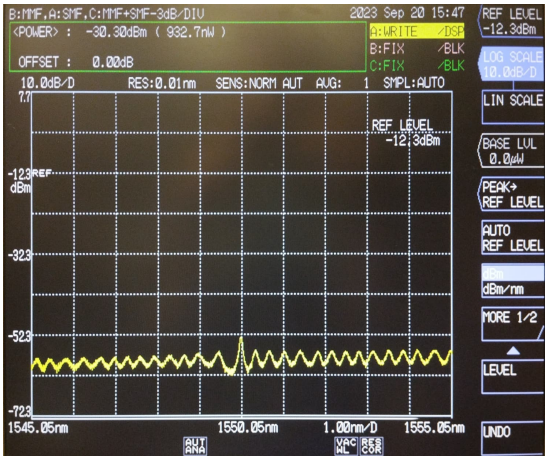


(b) $I = 30mA$

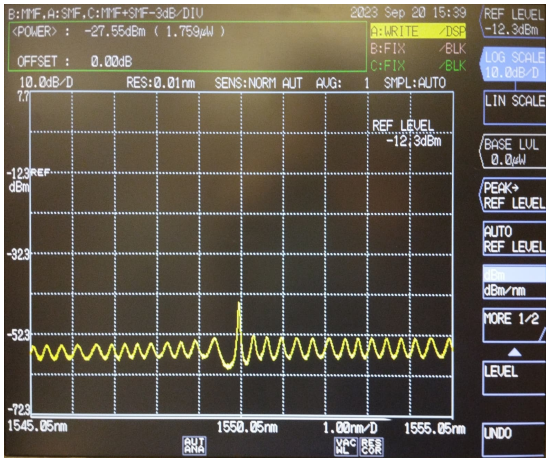


(c) $32.5mA$

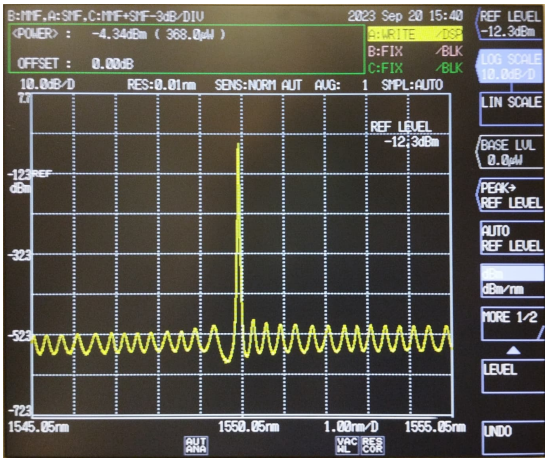


(d) $37.5mA$

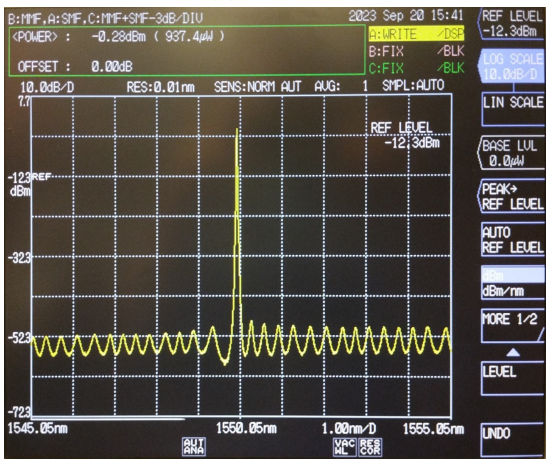


(e) $I = 42.5mA$

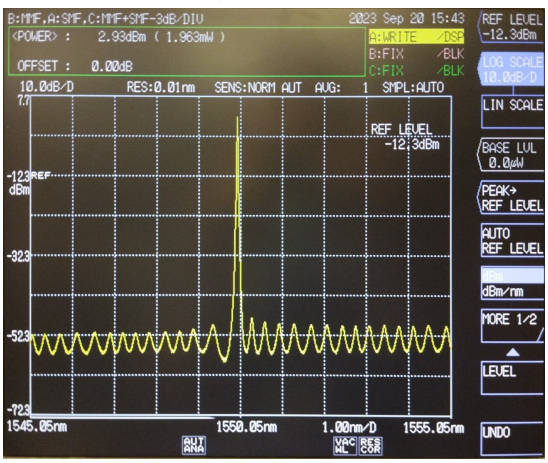


(f) $50mA$

Figure 3.3: Spectrum data for the DFB laser for various values of current, temperature fixed at 25.0°C

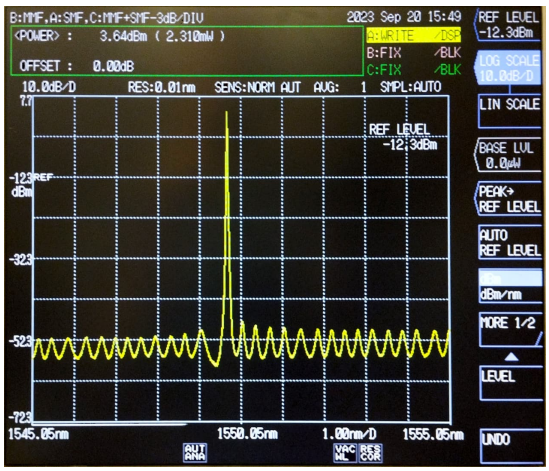


(a) $T = 22C$

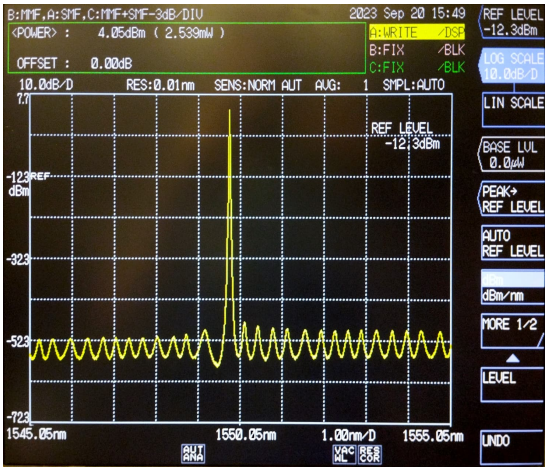


(b) $T = 23C$

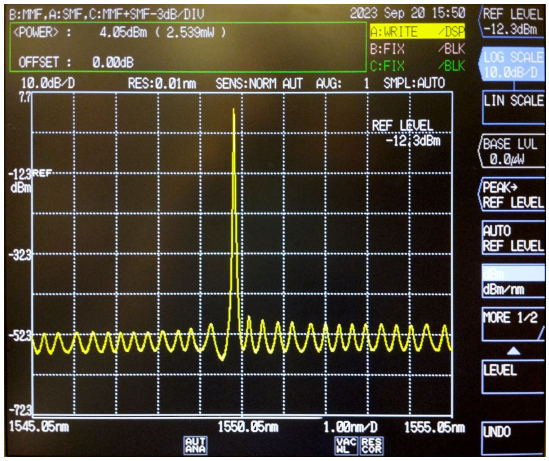


(c) $T = 24C$

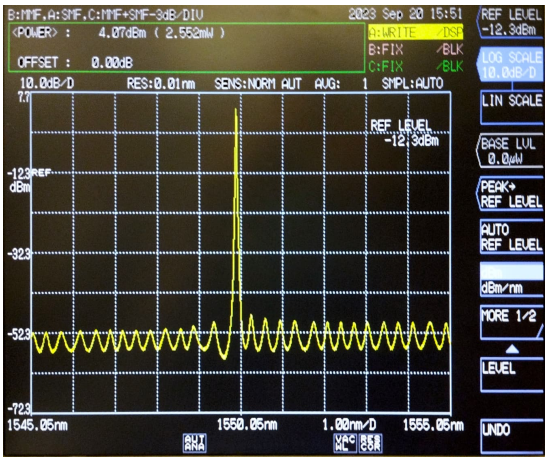


(d) $T = 25C$

Figure 3.4: Spectrum data for the DFB laser for various temperatures at a fixed current of 98.71mA

### 3.2.3 Discussion

The measured spectra confirmed the expected behavior for a DFB laser above and below the threshold current. Above the threshold, the central peak height increased rapidly with the applied current, while the other peaks did not change significantly, indicating lasing at a single wavelength. Below the threshold, the difference between the central peak and surrounding peaks was less pronounced, and the rate of increase of peak height was slower, in agreement with the LI curve.

A notable observation was the deep valleys around the peak wavelength in the OSA spectrum, especially before lasing (refer to 3.3b). This phenomenon, explained in literature, involves introducing an additional quarter-wavelength equivalent phase shift in the grating center. This shift results in a band-pass filter effect, focusing the transmission at the Bragg wavelength and causing the deep valley. Without this condition, achieving single-mode operation is challenging, as the laser tends to lase at two wavelengths on either side of the Bragg wavelength. As can be seen from the results of Soda and Imai [5]

Additionally, the data revealed a significant shift towards longer wavelengths at

higher temperatures (as shown in 3.4), a well-documented phenomenon in DFB lasers literature.[6] [7] This shift likely resulted from changes in the laser's cavity length and grating period due to thermal expansion, along with variations in the effective refractive index due to temperature fluctuations.

## 3.3 Characterisation of the Polarisation Controller

### 3.3.1 Procedure

The laser was connected to the polarisation controller, which went to the power meter.

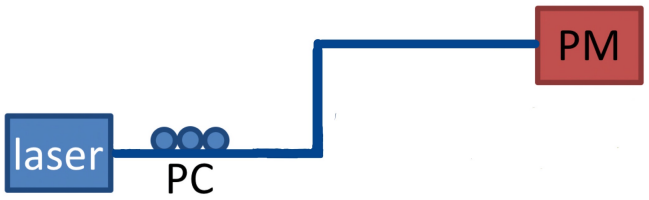


For a power of ~10dBm the insertion loss (input power minus output in dB) of the polarisation controller was measured while moving the paddles to change the polarisation state. The maximum and minimum losses were recorded.

### 3.3.2 Results

**Maximum Power Measured: 9.78dB**

**Minimum Power Measured: 9.74dB**

**Insertion loss of Polarisation Controller: 0.22dB**

### 3.3.3 Discussion

The calculated insertion loss of the polarisation controller was significiantly less than 1dB. There was little difference to the output power by moving the "bat ears" to change the polarisation state. The style of spherical power meter used was not very sensitive to polarisation.

## 3.4 Characterisation of the loss and polarisation extinction ratio of the modulator

### 3.4.1 Procedure

For this measurement, the output of the polarisation controller was connected to the input of the modulator, which was connected to the power meter.

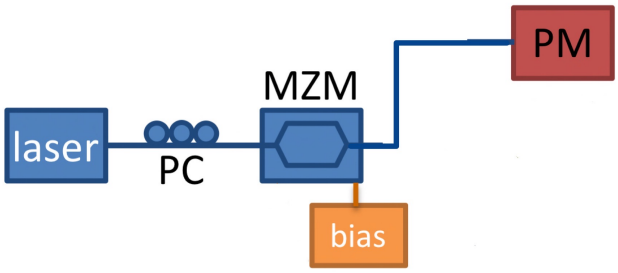


The polarisation state was varied as before, and the maximum and minimum insertion loss recorded. The measurement was carried out with a DC bias voltage of 5.4V on adivce of the supervisor. The extinction loss of the modulator was inferred from this.

### 3.4.2 Results

**Maximum Power Measured: 2.79dB Minimum Power Measured: -15.407dB**

### 3.4.3 Discussion

Subtracting the maximum measured power from 10 results in an insertion loss of 7.2dB, notably higher than the specified 3.2dB. However, at a DC bias of ~8.5V, the maximum power measured was 4.43mW (approximately 6.5dBm), corresponding to an insertion loss of 3.5dBm. Accounting for the polarization controller loss of ~0.22dBm and fiber coupling loss, the 3.2dBm specification is supported. The inferred extinction ratio is 18.2dB, slightly below the specified 20dBm but still close.

## 3.5 Measurement of Transfer Function

### 3.5.1 Procedure

In the experiment the DC bias voltage across the modulator was varied and the corresponding power readings taken. This data was plotted to create the modulator's transfer function. The transfer function was measured multiple times across both days to assess its time variability. One observed error was due to the apparatus being sensitive to polarization changes, likely due to loose fiber, as observed for the test transfer function generated on Day 1.

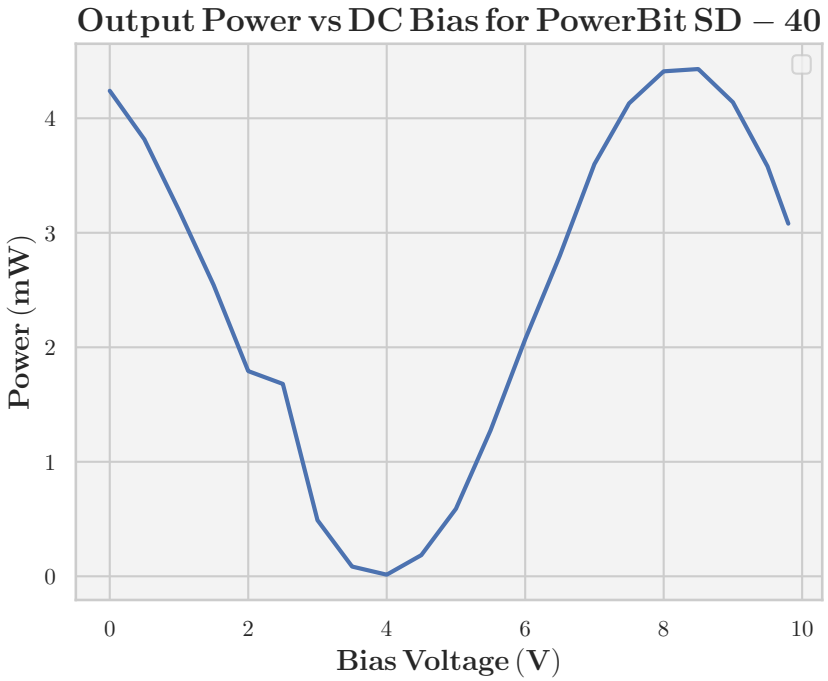


Figure 3.5: Test Transfer Function generated on day 1, there is clear deviation from the $cos^2(x)$ shape for the point at $V = 2.5V$ .

After securing loose fibers, the measurement was repeated, with reduced deviation from the expected shape.

### 3.5.2 Results

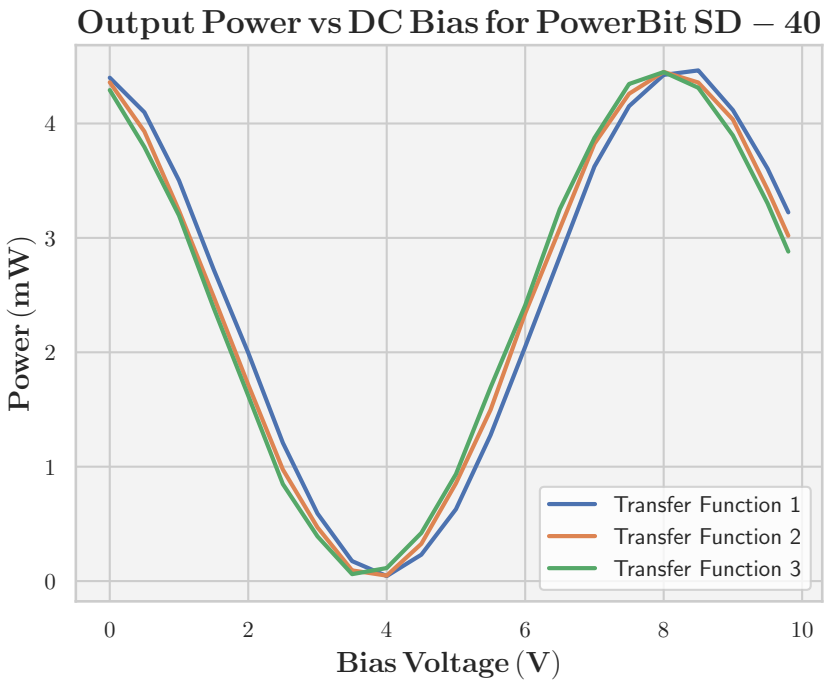


Figure 3.6: Three transfer functions measured in succession, (1 first, 3 last). Slight drift towards lower voltages observed

The estimated criticial points of the transfer function (max, min quadrature power) were

$$V_{max} \approx 8.6V$$

$$V_{min} \approx 4V$$

$$V_{quad} \approx 6.25V$$

During the experiment, it was observed that after adjusting the bias voltage, there was a subsequent rise in output power when the bias was around quadrature. As a result, the output power was measured over a span of five minutes both at quadrature, and at the maximum power ~8.5v

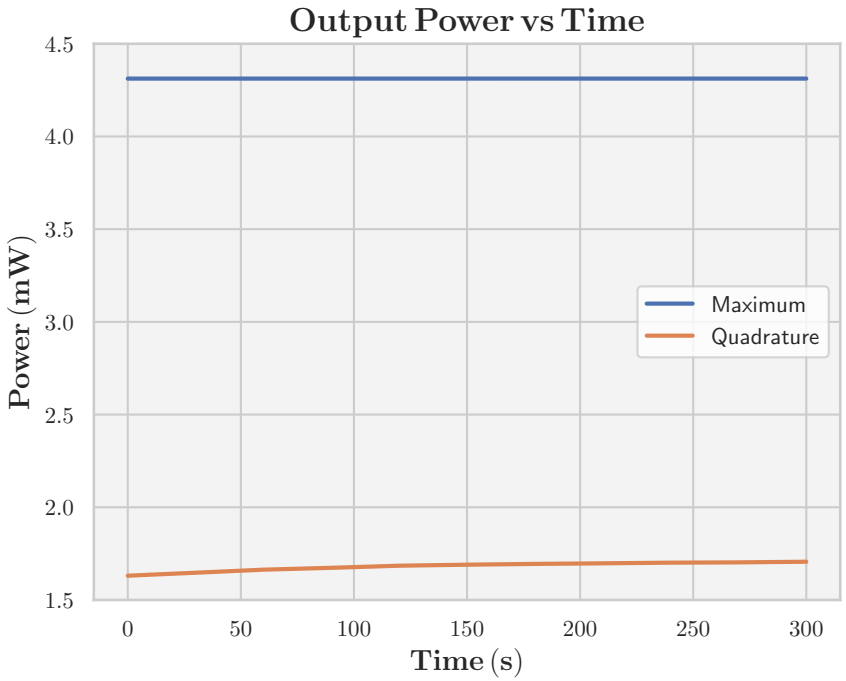


Figure 3.7: Power versus time at fixed current and temperature for two DC points of operation (Max and Quadrature at 6V). Larger increase in time was noted for the measurement at quadrature than that near the maximum

### 3.5.3 Discussion

The transfer function results align with the expected $cos^2(x)$ shape, with an estimated $V_\pi$ range of 4.5V (compared to the manual's 5.5V). However, due to sampling limitations (0.5V intervals), there's a potential error of ~0.5V in the $V_\pi$ value. (0.25V maximum error in each measurement)

A noticeable drift of ~0.5V occurred over a period of roughly forty minutes, as observed in fig 3.7. This drift explains the drift in power measured for a fixed current over 5 minutes, particularly at quadrature, where the rate of change of power w.r.t voltage is highest. It was stated in the manual that the Mach Zehnder modulator is sensitive to path length differences on the order of a wavelength, it is therefore possible that the drift is the result of thermal fluctuation altering the arm length of the MZM. To minimise this error, the MZM should be allowed to settle for a period before use.

## 3.6 Characterisation of Modulator Sine Wave Response

### 3.6.1 Procedure

The output of the modulator was connected to the 90-10 splitter (90 for photodetector, 10 for OSA)

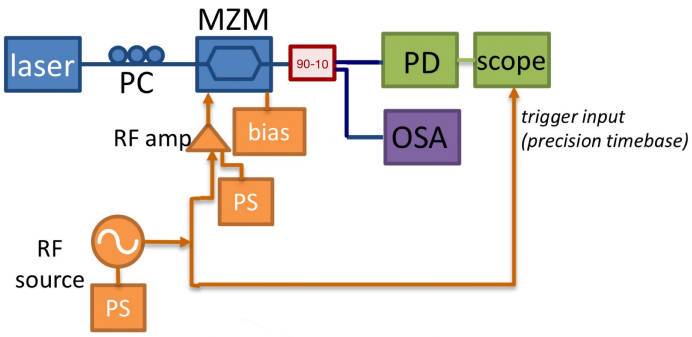


The procedure and safety guidelines for enabling the amplifiers and RF clock were observed at all times. These voltage limits were set by the demonstrator and were not altered throughout the lab.

After enabling the sine wave, the raw data, scope data and OSA data were collected, with the DC bias voltage set to achieve maximum, minimum and halfway power.

### 3.6.2 Results

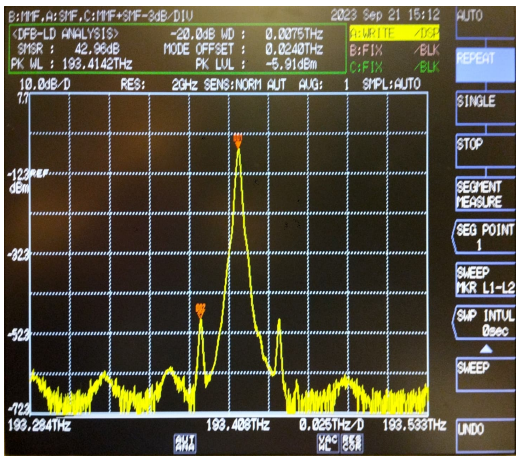


(a) *Spectrum Bias* 8.6*V* (*Max Power*)

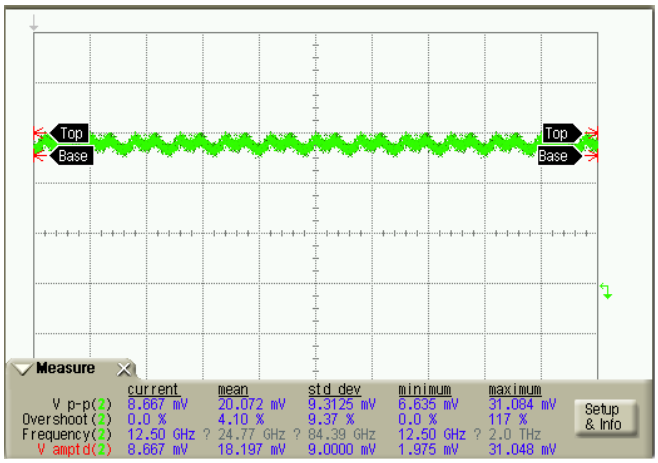


(b) *Scope Bias* 8.6*V* (*Max Power*)

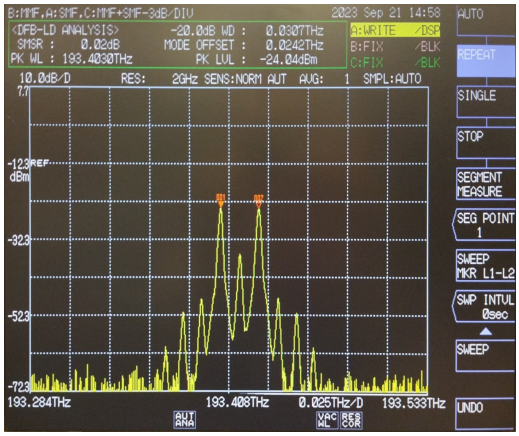


(c) *Spectrum Bias* 4*V* (*Min Power*)

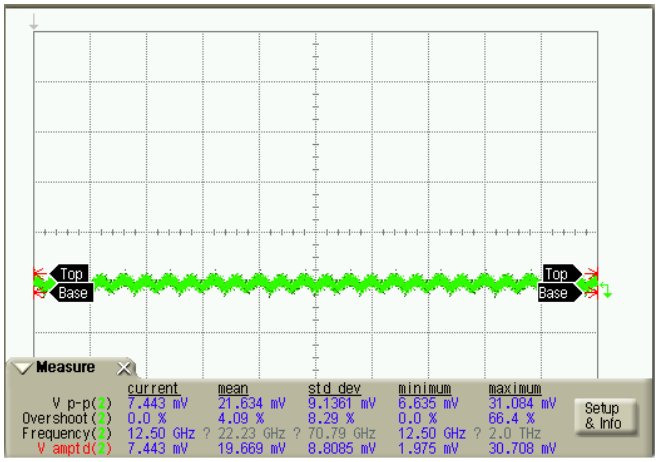


(d) *Scope Bias* 4*V* (*Min Power*)

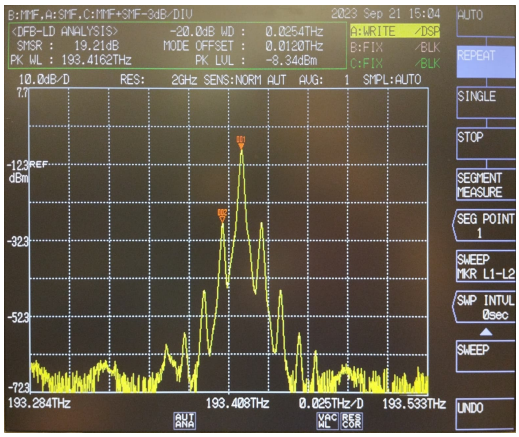


(e) *Spectrum Bias* 6*V* (*Quadrature*)

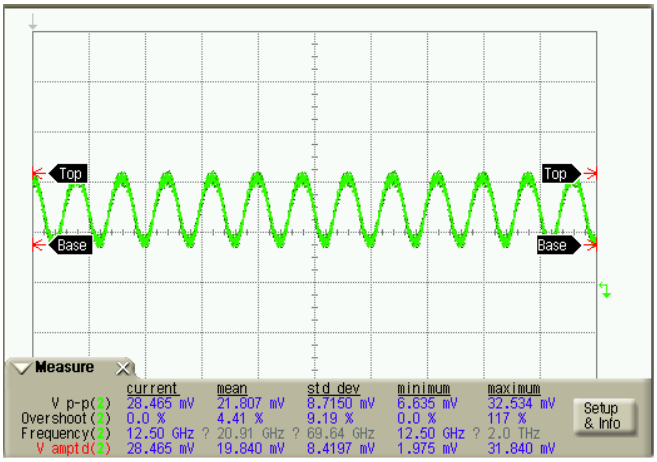


(f) *Scope Bias* 6*V* (*Quadrature*)

Figure 3.8: Spectrum and Scope Data for modulated signal with DC Bias at the three critical points of operation°C

### 3.6.3 Discussion

**Spectrum Data** Considering the spectrum, the observed behaviour is in line with the expectation of the theory presented in the fundamentals section. Sidebands are observed either side of the carrier evenly spaced in steps of the modulator frequency $f_m = 12.5GHz$. Changes to the bias voltage does not appear to affect the spacing. The DC bias does however impact the relative amplitudes of the various sidebands. The carrier frequency reaches maximum and minimum amplitude at the DC bias corresponding to maximum and minimum power from the transfer function. It was noted that at the bias corresponding to minimum power, the first order sideband dominates, and the third order sideband reaches a significant amplitude. This is in line with the results of Dar and Ahmad, which state that for an ideal Mach-Zehnder modulator, the optical output spectrum at minimum bias contains only odd-order sidebands, and in experiment they were shown to dominate at minimum transmission. [1]

**Scope Data** For the scope data, it was observed that at quadrature bias voltage, the mean frequency of the measured signal was 12.50GHz, the same as the applied signal. However at the maximum or minimum bias voltage, the mean frequency of the measured signal was ~22GHz, approximately double that of the applied signal. This can be understood in terms of the transfer function. Near a maximum or minimum of the transfer function, the $cos^2 x$ shape can be taylor approximated by a parabola.

$$I_0 cos^2(V_{max} + V_0 sin(2\pi f_c t) \propto (V_0 sin(2\pi f_c t))^2 \propto \frac{V_0}{2} - V_0 cos(2\pi(2fc_t))$$

We therefore expect the measured signal to have approximately twice the frequency of the applied signal, as was observed.

Near quadrature, assuming the swing of the modulating voltage is not too large, we can approximate the transfer function as a straight line, we then get the frequency of the measured signal to be approximately the same as the applied signal, as was observed.

## 3.7 Fourier Transform Analysis

The transforms of the raw scope data were calculated using SciPy.

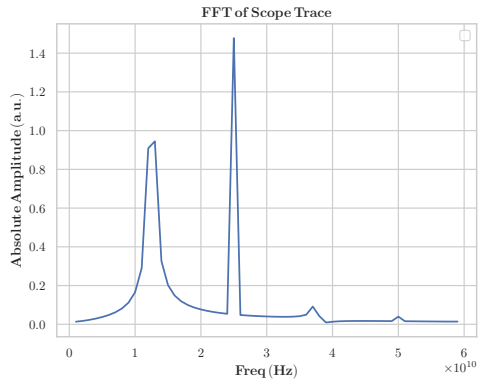


(a) *Bias* 8.6*V* (*Without DC*)

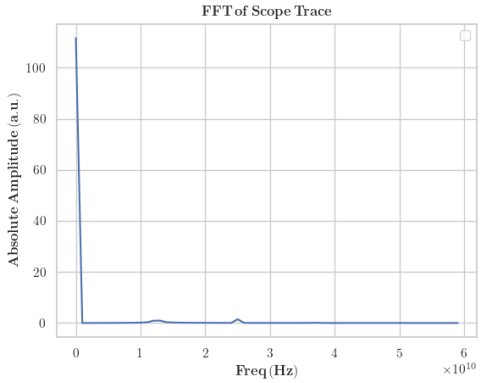


(b) *Bias* 8.6*V* (*With DC*)

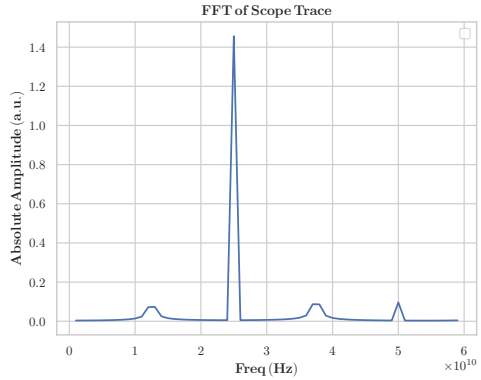


(c) *Bias* 4*V* (*Without DC*)

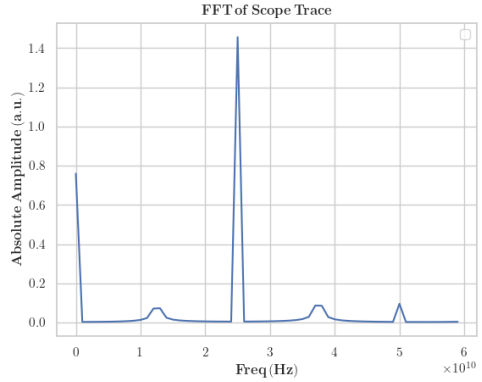


(d) *Bias* 4*V* (*With DC*)

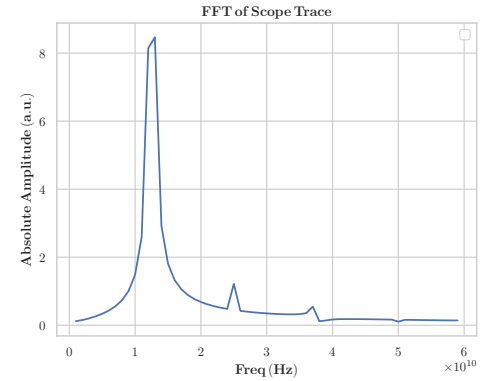


(e) *Bias* 6*V* (*Without DC*)

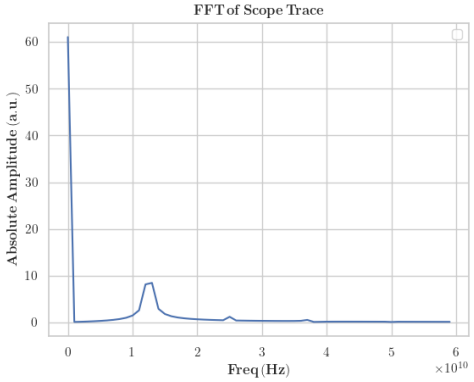


(f) *Bias* 6*V* (*With DC*)

Figure 3.9: Fourier Transforms from the Scope Data, plotted both with and without DC component so smaller peaks can be observed. The scale of the horizontal axis is 10GHz/div

As expected from the analysis of the scope data, for maximum and minimum bias, the dominant peak of the FFT is at 25GHz, twice the carrier frequency. While for the quadrature bias, the dominant peak is the one at 12.5GHz. Similar to the spectrum data, there are peaks evident at integer multiples of the modulator frequency. These are the result of $cos^2x$ shape of the transfer function, while it has been shown that around quadrature or at maximum or minimum bias, the full transfer function may be replaced by an approximation, however, away from the critical points of the trans-

fer function, for larger RF voltages, this may not be sufficient, and the full transfer function must be considered.

To this end, a simulation of the transfer function was created in Python. The transfer function was fitted to a $cos^2 x$ function. And the FFT could then be taken for different values of $V_{bias}$ and $V_0$, the RF voltage. The modulation frequency was let equal 1Hz for ease.

From these simulations it can be seen that near a maximum or minimum of the transfer function, the $2f_m$ term dominates even in the limit of large RF. Away from the maxima or minima, there are evenly spaced multiples of $f_m$, with decaying amplitude, as was observed in the spectral data. Interestingly, near 6V, the first and third harmonic dominate the second one, as was observed in the data from the OSA.

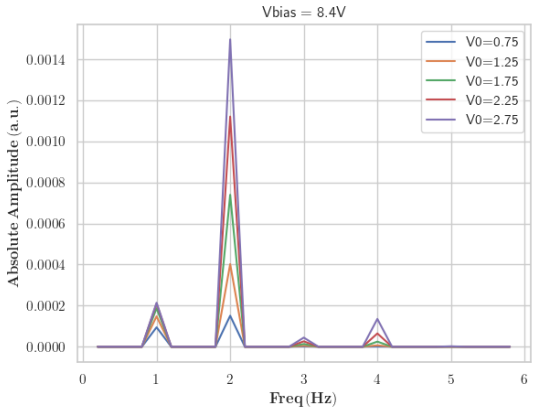


(a) Maximum DC Bias

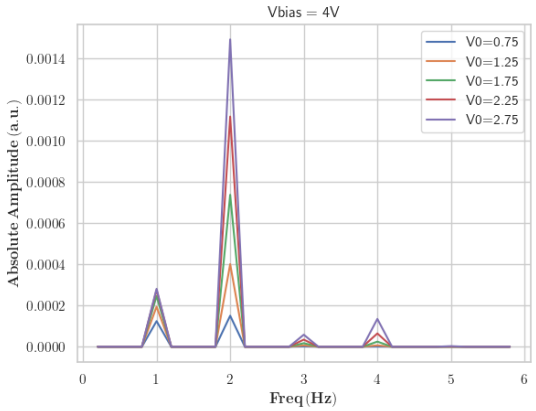


(b) Minimum DC Bias

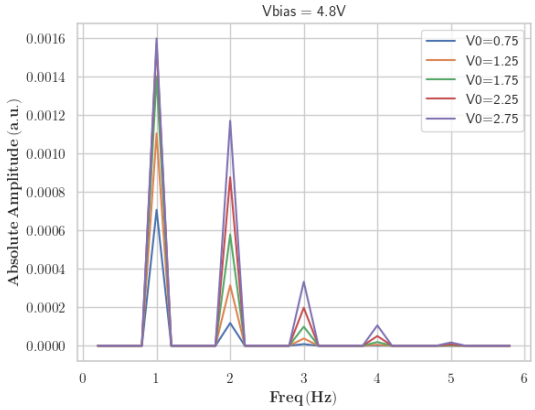


(c) 4.8V Bias (off center from minimum)

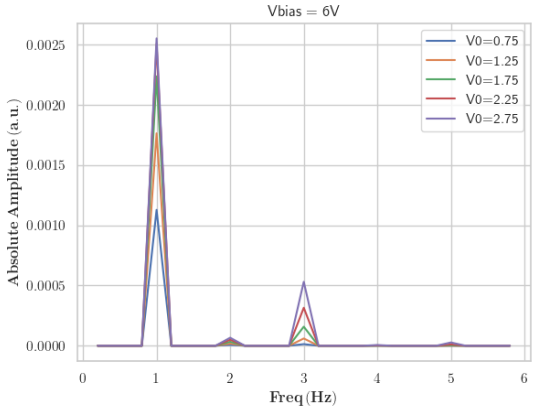


(d) Quadrature

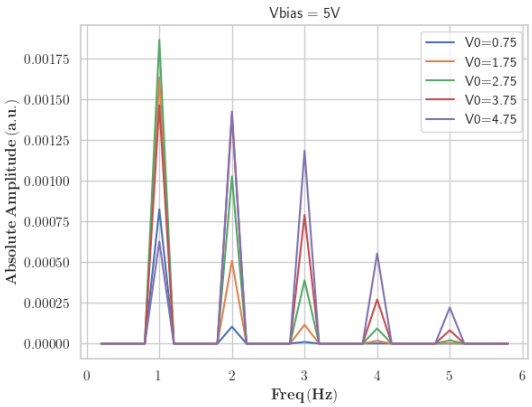


(e) Limit as RF frequency extends to cover transfer function

Figure 3.10: Fourier Transforms from the Python simulation, modulation frequency of 1Hz

# Chapter 4

# Conclusion

Overall, the experiment was a success. Many aspects of the MZM theory were verified, and the results agreed with previous experiments in the literature. Possible future directions for research would be to further investigate the behaviour of the modulator for bias away from the critical points. While it was outside of the scope of the report to speculate, there was strange assymetries noted between the spectrum at quadrature on the positive slope and that at the negative slope. It would be interesting to take more measurements at these points, and possibly to compare to a theoretical model for the behaviour away from the maxima.

It would also be interesting to take measurements of the optical output and time series data for modulation by a number of sine-wave components, to better observe some of the additional behvaiours and challenges coming from real data.

# Chapter 5

# Assessment of Learning

I really enjoyed this lab. Beforehand I was very unclear on what modulation was, having never studied it in depth. Performing real life characterisation of a modulator and attempting to understand the theory behind it cleared up a lot of the confusion I had, even outside of the realm of optical modualtors (e.g. AM/FM radio). It was also interesting to analyse the spectral data of the DFB laser. Performing this experiment has given me a good introduction to the field of signal processing, I find the combination of the physics of optics and photonics with attempting to encode real information very interesting.

# Bibliography


[1] A. B. Dar and F. Ahmad, "Realization of Mach-Zehnder Modulator with Ultra-high Extinction Ratio at Minimum Transmission Bias Point," 2020 IEEE 17th India Council International Conference (INDICON), New Delhi, India, 2020, pp. 1-5, doi: 10.1109/INDICON49873.2020.9342395.

[2] Abramowitz and I. A. Stegun, “Handbook of Mathematical Functions: With Formulas, Graphs, and Mathematical Tables,” In: M. Abramowitz and I. A. Stegun, Eds., Dover Books on Advanced Mathematics, Dover Publications, New York, 1965.

[3] G. R. Fowles, “Introduction to Modern Optics,” 2nd Edition, Dover Publications, Inc., New York, 1989.

[4] S. H. Simon, "The Oxford Solid State Basics", 1st Edition, Oxford University Press, Oxford, 2013

[5] H. Soda and H. Imai, "Analysis of the spectrum behavior below the threshold in DFB lasers," in IEEE Journal of Quantum Electronics, vol. 22, no. 5, pp. 637-641, May 1986, doi: 10.1109/JQE.1986.1073020.

[6] Jingsi Li, Huan Wang, Xiangfei Chen, Zuowei Yin, Yuechun Shi, Yanqing Lu, Yitang Dai, and Hongliang Zhu, "Experimental demonstration of distributed feedback semiconductor lasers based on reconstruction-equivalent-chirp technology," Opt. Express 17, 5240-5245 (2009)

[7] International Journal of Optoelectronic Engineering p-ISSN: 2167-7301 e-ISSN: 2167-731X 2015; 5(2): 21-27 doi:10.5923/j.ijoe.20150502.01